Oscillating Incompressible Aerodynamics of a Loaded Airfoil Cascade

Hsiao-Wei D. Chiang* and Sanford Fleeter†
Purdue University, West Lafayette, Indiana

A complete first order model is developed to predict the oscillating incompressible aerodynamics of an airfoil cascade, including the effects of steady loading. The cascade steady and unsteady flowfields are analyzed by considering a periodic flow channel. The velocity potential is separated into steady and unsteady harmonic components, each of which is described by a Laplace equation. An analytical solution in individual grid elements of a body-fitted computational grid is then determined, with the complete solution obtained by assembling these local solutions. The capabilities and validity of this model and solution technique are demonstrated by considering the steady and unsteady aerodynamics of both theoretical and experimental cascade configurations.

Nomenclature

b = airfoil semichord, $C/2$
$\bar{C}_p$ = steady surface static pressure, $p/\frac{1}{2}\rho U_\infty^2$
C_p = unsteady pressure difference, $\Delta p/\rho U_\infty^2 \bar{\alpha}$
k = reduced frequency, $\omega b/U_\infty$
U_∞ = steady farfield flow
U_0 = steady airfoil surface chordwise velocity
V_0 = steady airfoil surface normal velocity
x_0 = elastic axis location
α_0 = mean incidence angle
$\bar{\alpha}$ = amplitude of torsional oscillations
β_0 = interblade phase angle
θ = inlet blade angle
Φ = general velocity potential
Φ_0 = steady velocity potential
Φ' = unsteady velocity potential
Φ'_C = circulatory unsteady velocity potential
Φ'_{NC} = noncirculatory unsteady velocity potential
Γ = steady circulation constant
Γ' = unsteady circulation constant
ω = oscillatory frequency

Introduction

TO predict the susceptibility of turbomachine blade rows to aeroelastic problems, the unsteady aerodynamics of a harmonically oscillating airfoil cascade must be determined. Typically, these unsteady aerodynamic calculations are based on thin airfoil theory, with the blade row modeled as an infinite cascade of flat-plate airfoils executing small perturbation harmonic oscillations at zero incidence in a uniform and parallel steady flow. The unsteady flowfield is thus uncoupled from the steady flow. The linearized unsteady aerodynamics of the oscillating cascade are then calculated, using standard mathematical and numerical techniques.

In turbomachines, however, cascaded airfoils with nonzero mean flow incidence, arbitrary shape, and large camber must be considered. Hanamura[1,2] accounted for the effect of camber by considering circular arc airfoils. Also, Atassi and Akai[3] developed an analysis for a cascade comprised of airfoils with moderate camber oscillating in a uniform incompressible flowfield. These unsteady aerodynamic models utilize classical airfoil techniques, resulting in analytical solutions in the form of integral equations for the unsteady lift. Although such classical models and integral solution techniques are certainly important, the development and use of computers and numerical methods enables the mathematical modeling to be extended and enhanced.

In this paper, a complete first-order model is developed, i.e., the thin airfoil approximation is not utilized, to analyze the oscillating incompressible aerodynamics of an airfoil cascade, including steady aerodynamic loading. In particular, airfoil profile, cascade geometry, and mean flow incidence angle effects are considered. The cascade steady and unsteady flowfields are analyzed by considering a single flow channel with periodic boundary conditions. The fluctuating flow velocity is assumed to be small compared to the steady flow. The velocity potential is separated into steady and unsteady harmonic parts, with both the steady and unsteady potential further decomposed into circulatory and noncirculatory components. These velocity potentials are individually described by Laplace equations. The steady velocity potential is independent of the unsteady flowfield. However, the unsteady flow is coupled to the steady flowfield through the boundary conditions on the surfaces of the oscillating airfoils.

A locally analytical solution is developed in which the discrete alegebraic equations which represent the flowfield equations are obtained from analytical solutions in individual elements of a body-fitted computational grid. General analytical solutions to the transformed Laplace equations are developed by applying these solutions to individual grid elements, with the complete flowfield then obtained by assembling these locally analytical solutions.

The locally analytical method for steady two-dimensional fluid flow and heat transfer problems was initially developed by Chen et al.[4-7] They have shown that the locally analytical method has several advantages over the finite-difference and finite-element methods. For example, it is less dependent on grid size and the system of algebraic equations is relatively stable. Also, since the solution is analytical, it is differentiable and is a continuous function in the solution domain. The disadvantage is that a great deal of mathematical analysis is required before programming.

Mathematical Model

Figure 1 schematically depicts the two-dimensional flow past a cascade comprised of thick, cambered airfoils that are

Received Dec. 14, 1987; revision received May 13, 1988.

*Graduate Research Assistant, Thermal Sciences and Propulsion Center. Student Member AIAA.

†Professor, School of Mechanical Engineering, and Director, Thermal Sciences and Propulsion Center. Associate Fellow AIAA.

executing torsion mode oscillations. Also shown is the nondimensional Cartesian coordinate system. The steady and uniform farfield flow is specified by the velocity vector U_∞, with the mean incidence angle to the airfoil cascade denoted by α_0. The cascade stagger angle is denoted by δ, with S the distance between the airfoils along the stagger line and θ the inlet blade angle.

For an incompressible unsteady inviscid fluid, a velocity potential function can be defined. The complete flowfield is then described by a Laplace equation:

$$\nabla^2\Phi=0 \tag{1}$$

where $\Phi=\Phi(x,y,t)$ is the velocity potential.

Since the Laplace equation is linear, the velocity potential can be decomposed into components by the superposition principle. In particular, the velocity potential is decomposed into steady and unsteady components, $\Phi_0(x,y)$ and $\Phi'(x,y,t)$. The steady potential is further decomposed into noncirculatory and circulatory components, $\Phi_{NC}(x,y)$ and $\Phi_C(x,y)$. The unsteady potential is assumed to have an harmonic time dependence of frequency ω, and is also decomposed into noncirculatory and circulatory components, $\Phi'_{NC}(x,y)$, $\Phi'_C(x,y)$:

$$\Phi(x,y,t)=[\Phi_{NC}(x,y)+\Gamma\Phi_C(x,y)]+e^{ikt}[\Phi'_{NC}(x,y)+\Gamma'\Phi'_C(x,y)] \tag{2}$$

where $\nabla^2\Phi_{NC}=0$; $\nabla^2\Phi_C=0$; $\nabla^2\Phi'_{NC}=0$; $\nabla^2\Phi'_C=0$; Γ and Γ' are the unknown steady and unsteady flow circulation constants, and k is the reduced frequency, $k=\omega b/U_\infty$.

To complete the mathematical model, farfield inlet, farfield exit, airfoil surface, wake dividing streamline, and cascade periodic boundary conditions must be specified for the four velocity potential functions, $\Phi_{NC}(x,y)$, $\Phi_C(x,y)$, $\Phi'_{NC}(x,y)$, and $\Phi'_C(x,y)$.

At the farfield inlet boundary, the flow is steady and uniform, with the velocity potential boundary conditions given in Eqs. (3):

$$\Phi_{NC}|_{\text{farfield inlet}}=|U_\infty|x \tag{3a}$$

$$\Phi_C|_{\text{farfield inlet}}=0 \tag{3b}$$

$$\Phi'_{NC}|_{\text{farfield inlet}}=-\left|\frac{S}{\beta_0}\right|\left.\frac{\partial\Phi'_{NC}}{\partial n}\right|_{\text{farfield inlet}} \tag{3c}$$

$$\Phi'_C|_{\text{farfield inlet}}=-\left|\frac{S}{\beta_0}\right|\left.\frac{\partial\Phi'_C}{\partial n}\right|_{\text{farfield inlet}} \tag{3d}$$

where β_0 is the interblade phase angle, and n is the surface unit normal.

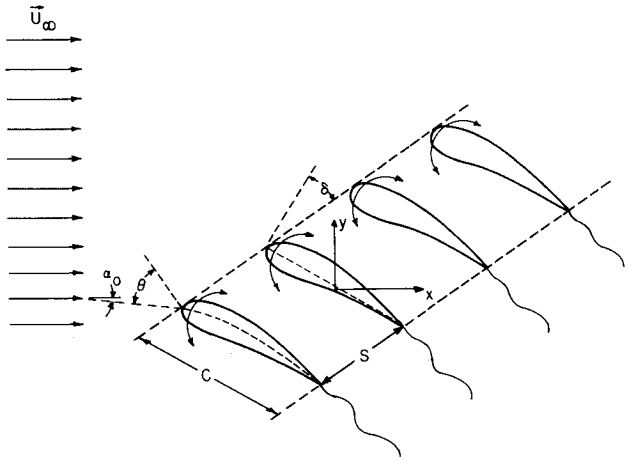

Fig. 1 Flowfield schematic.

At the farfield exit boundary, the velocity potential boundary conditions are given in Eqs. (4):

$$\left.\frac{\partial\Phi_{NC}}{\partial n}\right|_{\text{farfield exit}}=|U_\infty|\cos(\alpha_0+\theta) \tag{4a}$$

$$\left.\frac{\partial\Phi_C}{\partial n}\right|_{\text{farfield exit}}=0 \tag{4b}$$

$$\Phi'_{NC}|_{\text{farfield exit}}=-\left|\frac{S}{\beta_0}\right|\left.\frac{\partial\Phi'_{NC}}{\partial n}\right|_{\text{farfield exit}} \tag{4c}$$

$$\Phi'_C|_{\text{farfield exit}}=-e^{-ikx}\left(\frac{e^{ky}}{1-\exp[(k-i\nu)S\cos\delta]}+\frac{e^{-ky}}{1-\exp[-(k+i\nu)S\cos\delta]}\right) \tag{4d}$$

where $\nu=(\beta_0+k\sin\delta/S)/S\cos\delta$.

The airfoil surface boundary conditions specify that the normal velocity of the flowfield must be equal to that of the airfoil:

$$\left.\frac{\partial\Phi_{NC}}{\partial n}\right|_{\text{airfoil}}=0 \tag{5a}$$

$$\left.\frac{\partial\Phi_C}{\partial n}\right|_{\text{airfoil}}=0 \tag{5b}$$

$$\left.\frac{\partial\Phi'_C}{\partial n}\right|_{\text{airfoil}}=0 \tag{5c}$$

$$\left.\frac{\partial\Phi'_{NC}}{\partial n}\right|_{\text{airfoil}}=W'(x,y) \tag{5d}$$

The normal velocity boundary condition being applied on the mean position of the airfoil, $W'(x,y)$, is a function of both the position of the airfoil and the steady flowfield. Thus, it is the boundary condition that couples the unsteady flowfield to the steady aerodynamics. For an airfoil cascade executing harmonic torsion mode oscillations about an elastic axis location at x_0, as measured from the leading edge, the normal velocity on the surfaces of the airfoil is defined in Eq. (6):

$$W'(x,y)=\bar{\alpha}e^{i\beta_0}\left[\frac{ik[(x-x_0)+y\partial f/\partial x]+U_0+V_0\partial f/\partial x}{[1+(\partial f/\partial x)^2]^{1/2}}+\frac{\partial U_0/\partial y[(x-x_0)\partial f/\partial x+y]}{[1+(\partial f/\partial x)^2]^{1/2}}-\frac{\partial V_0/\partial y[(x-x_0)-y\partial f/\partial x]}{[1+(\partial f/\partial x)^2]^{1/2}}\right] \tag{6}$$

where $U_0=U_0(x,y)$ and $V_0=V_0(x,y)$ are the steady velocity components, $f(x)$ denotes the airfoil profile, and $\bar{\alpha}$ is the amplitude of the torsional ocillations.

The steady and unsteady velocity potentials are both discontinuous along the airfoil wake dividing streamline. The steady flow discontinuity is satisfied with a continuous noncirculatory velocity potential and a discontinuous circulatory velocity potential. The steady circulatory velocity potential discontinuity is equal to the steady circulation Γ [Eqs. (7)]. Also specified is the continuity of the steady noncirculatory velocity potential along the wake streamline:

$$\Delta\Phi_C|_{\text{wake}}=\Phi_C^+-\Phi_C^-=\Gamma=\Delta\Phi_C|_{TE} \tag{7a}$$

$$\Delta\Phi_{NC}|_{\text{wake}}=0 \tag{7b}$$

where *TE* denotes the airfoil trailing edge, and the superscripts plus and minus denote the upper and lower airfoil surfaces, respectively.

The unsteady flow discontinuity is also satisfied with a continuous noncirculatory velocity potential and a discontinuous circulatory velocity potential. The unsteady circulatory velocity potential discontinuity is specified by requiring the pressure to be continuous across the wake and then utilizing the unsteady Bernoulli equation to relate the unsteady velocity potential and the pressure. The resulting circulatory potential wake streamline discontinuity is given in Eqs. (8). Also specified is the continuity of the noncirculatory velocity potential along the wake streamline:

$$\Delta\Phi_C' \mid_{\text{wake}} = \Gamma' \exp\{-ik(x-1)\} \tag{8a}$$

$$\Delta\Phi_{NC}' \mid_{\text{wake}} = 0 \tag{8b}$$

In addition, the Kutta condition is applied to both the steady and the unsteady flowfields. This enables the steady and unsteady circulation constants, Γ and Γ', to be determined. For the steady flowfield, the Kutta condition is satisfied by requiring the chordwise velocity components on the upper and lower airfoil surfaces to be equal in magnitude at the trailing edge:

$$\mid U_0 \mid_{TE}^{+} = \mid U_0 \mid_{TE}^{-} \tag{9}$$

The Kutta condition is imposed on the unsteady potential flowfield by requiring no unsteady pressure difference across the airfoil chordline at the trailing edge. The corresponding relation for the trailing edge unsteady velocity potential difference is determined from the unsteady Bernoulli equation:

$$\Delta P' \mid_{TE} = P' \mid_{TE}^{+} - P' \mid_{TE}^{-} = 0 \tag{10a}$$

$$[\nabla\Phi_0 \cdot \nabla\Phi' + ik\Phi'] \mid_{TE}^{+} = [\nabla\Phi_0 \cdot \nabla\Phi' + ik\Phi'] \mid_{TE}^{-} \tag{10b}$$

The velocity potential boundary conditions on the cascade periodic boundaries are given in Eqs. (11):

$$\Phi_{NC} \mid_{\text{upper boundary}} = \Phi_{NC} \mid_{\text{lower boundary}} + \mid U_\infty \mid S \sin(\alpha_0 + \theta) \tag{11a}$$

$$\left.\frac{\partial\Phi_{NC}}{\partial s}\right|_{\text{upper boundary}} = -\left.\frac{\partial\Phi_{NC}}{\partial s}\right|_{\text{lower boundary}} \tag{11b}$$

$$\Phi_C \mid_{\text{upper boundary}} = \Phi_C \mid_{\text{lower boundary}} \tag{11c}$$

$$\left.\frac{\partial\Phi_C}{\partial s}\right|_{\text{upper boundary}} = -\left.\frac{\partial\Phi_C}{\partial s}\right|_{\text{lower boundary}} \tag{11d}$$

$$\Phi_{NC}' \mid_{\text{upper boundary}} = e^{i\beta_0} \Phi_{NC}' \mid_{\text{lower boundary}} \tag{11e}$$

$$\left.\frac{\partial\Phi_{NC}'}{\partial s}\right|_{\text{upper boundary}} = e^{i\beta_0} \left.\frac{\partial\Phi_{NC}'}{\partial s}\right|_{\text{lower boundary}} \tag{11f}$$

$$\Phi_C' \mid_{\text{upper boundary}} = e^{i\beta_0} \Phi_C' \mid_{\text{lower boundary}} \tag{11g}$$

$$\left.\frac{\partial\Phi_C'}{\partial s}\right|_{\text{upper boundary}} = e^{i\beta_0} \left.\frac{\partial\Phi_C'}{\partial s}\right]_{\text{lower boundary}} \tag{11h}$$

where s is the unit vector along the stagger line direction.

The unsteady dependent variable of primary interest is the unsteady pressure. This is determined from the solution for the steady flowfield, the unsteady velocity potential, and the unsteady Bernoulli equation. Also, the unsteady airfoil surface boundary conditions were applied on the mean position of the airfoil [Eq. (6)]. After transfer to the instantaneous airfoil position, the unsteady pressure becomes

$$p' = -\nabla\Phi_0 \cdot \nabla\Phi' - ik\Phi' + \frac{\partial U_0}{\partial y}(-U_0 x + V_0 y) - \frac{\partial V_0}{\partial y}(V_0 x + U_0 y) \tag{12}$$

where the last two terms account for the transfer of the pressure value from the mean position of the airfoil to its instantaneous position.

Computational Domain

Computational Grid

A boundary-fitted computational grid-generation technique is utilized for the numerical solution.[8] A Poisson grid solver is used to fit a C-type grid to the flow passage of a typical airfoil in the cascade. This method permits grid points to be specified along the entire boundary of the computational plane. As depicted in Fig. 2, the boundary in the physical plane is denoted by the curve *abcdefghia* and encompasses the airfoil, its wake, the farfield inlet, the farfield exit, and the cascade periodic boundaries. The application of this grid generation technique results in an equally spaced, orthogonal computational grid at the interior points in the transformed (ξ,η) plane. Attractive features of this technique include mesh clustering in regions of high surface curvature; high grid orthogonality, especially in the near airfoil surface and periodic boundary regions; and the establishment of periodic grids for ease of enforcing cascade periodic boundary conditions. A typical boundary-fitted grid for a Gostelow airfoil cascade is shown in Fig. 3.

Laplace equations describe the complete flowfield, including the unknown velocity potentials Φ_{NC}, Φ_C, Φ_{NC}', and Φ_C' [Eq. (2)]. In the transformed (ξ,η) coordinate system, the Laplace equation takes on the following nonhomogeneous form:

$$\frac{\partial^2\Phi}{\partial\xi^2} + \alpha\frac{\partial^2\Phi}{\partial\eta^2} - 2\alpha\beta\frac{\partial\Phi}{\partial\eta} - 2\gamma\frac{\partial\Phi}{\partial\xi} = F(\xi,\eta) \tag{13}$$

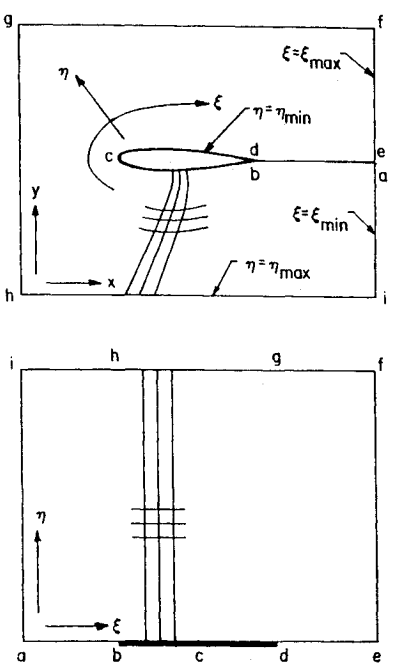

Fig. 2 Body-fitted coordinate transformation.

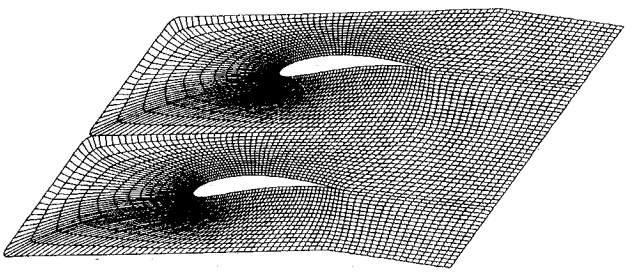

Fig. 3 Computational grid for Gostelow airfoil cascade.

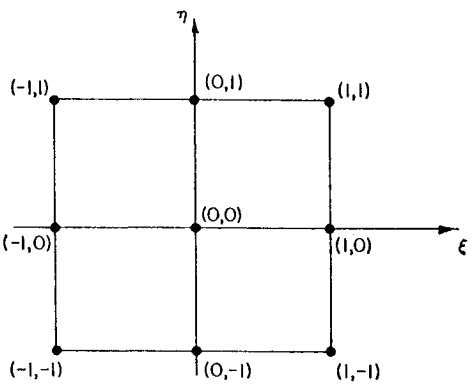

Fig. 4 Local computational grid element.

where Φ is a shorthand method of writing these four velocity potentials in the transformed plane, i.e., Φ denotes $\Phi_{NC}(\xi,\eta)$, $\Phi_C(\xi,\eta)$, $\Phi'_{NC}(\xi,\eta)$, or $\Phi'_C(\xi,\eta)$; $F(\xi,\eta)$ contains the cross-derivative term $\partial^2\Phi/\partial\xi\,\partial\eta$, and the coefficients α, β, and γ are functions of the transformed coordinates ξ and η that are treated as constants in each individual grid element.

Analytical Solution

To obtain the analytical solution to the transformed Laplace equation, it is first rewritten as a homogeneous equation by defining a new dependent variable $\tilde{\phi}(\xi,\eta)$:

$$\frac{\partial^2\tilde{\phi}}{\partial\xi^2}+\alpha\frac{\partial^2\tilde{\phi}}{\partial\eta^2}-(\gamma^2+\alpha\beta^2)\tilde{\phi}=0 \tag{14}$$

where

$$\Phi=\tilde{\phi}\exp\{\gamma\xi+\beta\eta\}-\frac{F(\gamma\xi+\beta\eta)}{2(\gamma^2+\alpha\beta^2)}$$

The general solution for $\tilde{\phi}$ is determined by separation of variables and is given in Eq. (15):

$$\tilde{\phi}(\xi,\eta)=[A_1\cos(\lambda\xi)+A_2\sin(\lambda\xi)]\times[B_1\cos(\mu\eta)+B_2\sin(\mu\eta)] \tag{15}$$

where $\mu=[(\gamma^2+\alpha\beta^2+\lambda^2)/\alpha]^{1/2}$, and λ, A_1, A_2, B_1, and B_2 are constants to be determined from the boundary conditions.

Locally Analytical Solution

Analytical solutions in individual computational grid elements are determined by applying proper boundary conditions on each element to evaluate the unknown constants in the general velocity potential solution specified in Eq. (15). The solution to the global problem is then determined through the application of the global boundary conditions and the assembly of the locally analytical solutions.

Grid Element Boundary Conditions

A typical computational grid element is schematically depicted in Fig. 4. The local element boundary conditions specify the values of the various velocity potentials at the eight boundary nodal points. However, to obtain unique analytical solutions to the Laplace equation in this element, i.e., determine the values of the integration constants in the general solution for each element, continuous boundary conditions are required on all four boundaries. For numerical purposes, these boundary conditions are expressed in an implicit formulation in terms of the three known nodal values on each element boundary. In particular, a combination of a linear and exponential function [Eqs. (16)] are utilized on each boundary as they satisfy the Laplace equation:

$$\tilde{\phi}(\xi,1)=a_1^{(1)}\exp\{\xi\}+a_2^{(1)}\xi+a_3^{(1)} \tag{16a}$$

$$\tilde{\phi}(1,\eta)=a_1^{(2)}\exp\{\eta\}+a_2^{(2)}\eta+a_3^{(2)} \tag{16b}$$

$$\tilde{\phi}(\xi,-1)=a_1^{(3)}\exp\{\xi\}+a_2^{(3)}\xi+a_3^{(3)} \tag{16c}$$

$$\tilde{\phi}(-1,\eta)=a_1^{(4)}\exp\{\eta\}+a_2^{(4)}\eta+a_3^{(4)} \tag{16d}$$

where the constants $a_1^{(i)}$, $a_2^{(i)}$, and $a_3^{(i)}$ are determined from the known values at the three nodal points on each boundary.

Grid Element Analytical Solutions

The general analytical solution to the Laplace equation given in Eq. (15) is valid in individual grid elements as well as over the complete flow region. To determine the relationship between the velocity potential at the center of the typical grid element (Fig. 4) and its surrounding values, the superposition principle is used to decompose the solution for $\tilde{\phi}$ into four components, each having only one nonhomogeneous boundary condition:

$$\begin{aligned}\tilde{\phi}(\xi,\eta)=\sum_{n=1}^{\infty}\{&A_{n1}\sinh[\mu_n(\eta+1)]\sin[\lambda_n(\xi+1)]\\&+A_{n2}\sinh[\mu_n(\eta-1)]\sin[\lambda_n(\xi+1)]\\&+A_{n3}\sinh[\mu'_n(\xi+1)]\sin[\lambda_n(\eta+1)]\\&+A_{n4}\sinh[\mu'_n(\xi-1)]\sin(\lambda_n(\eta+1)]\}\end{aligned} \tag{17}$$

where $\lambda_n=n\pi/2$; $\mu_n=[(\gamma^2+\beta^2\alpha+\lambda_n^2)/\alpha]^{1/2}$; $\mu'_n=(\gamma^2+\beta^2\alpha+\lambda_n^2\alpha)^{1/2}$.

The application of the local boundary conditions [Eqs. (16)], together with the orthogonality of the Fourier series, leads to the following values for A_{ni}:

$$\begin{aligned}A_{ni}=&C_{1ni}\tilde{\phi}(1,1)+C_{2ni}\tilde{\phi}(1,0)+C_{3ni}\tilde{\phi}(1,-1)\\&+C_{4ni}\tilde{\phi}(0,-1)+C_{5ni}\tilde{\phi}(-1,-1)+C_{6ni}\tilde{\phi}(-1,0)\\&+C_{7ni}\tilde{\phi}(-1,1)+C_{8ni}\tilde{\phi}(0,1)\end{aligned} \tag{18}$$

where the constants $C_{1ni}\ldots$, C_{8ni} are functions of the $a_1^{(i)}$, $a_2^{(i)}$, and $a_3^{(i)}$ boundary constants.

With the analytical solution in an individual grid element thus specified, [Eqs. (17) and (18)], the value of $\tilde{\phi}$ at the center of the element can be written as follows:

$$\begin{aligned}\tilde{\phi}(0,0)=\sum_{n=1}^{\infty}\{&[(A_{n1}-A_{n2})\sinh(\mu_n)\\&+(A_{n3}-A_{n4})\sinh(\mu'_n)]\sin(\lambda_n)\}\end{aligned} \tag{19}$$

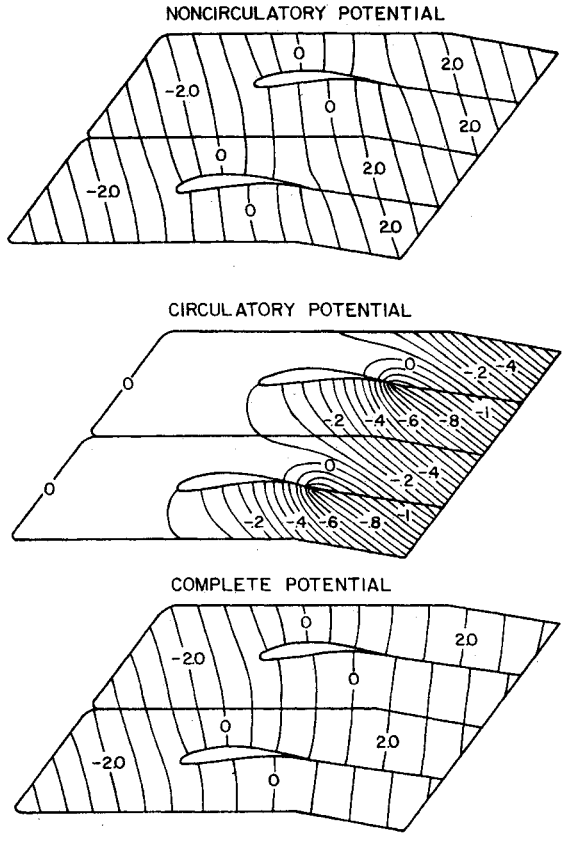

Fig. 5 Gostelow cascade velocity potentials.

Substituting for the A_{ni} terms [Eq. (18)] leads to the following:

$$\tilde{\phi}(0,0) = C_1'\tilde{\phi}(1,1) + C_2'\tilde{\Phi}(1,0) + C_3'\tilde{\phi}(1,-1) + C_4'\tilde{\phi}(0,-1) + C_5'\tilde{\phi}(-1,-1) + C_6'\tilde{\phi}(-1,0) + C_7'\tilde{\phi}(-1,1) + C_8'\tilde{\phi}(0,1) \quad (20)$$

where the constants C_1', C_2', ..., C_i' are functions of the $a_1^{(i)}$, $a_2^{(i)}$, and $a_3^{(i)}$ boundary constants, as well as of the transformed coordinate functions α, β, and γ.

This solution for $\tilde{\phi}$ at the center point is rewritten in terms of the original dependent variable Φ in Eqs. (21):

$$\Phi(0,0) = C_1\Phi(1,1) + C_2\Phi(1,0) + C_3\Phi(1,-1) + C_4\Phi(0,-1) + C_5\Phi(-1,-1) + C_6\Phi(-1,0) + C_7\Phi(-1,1) + C_8\Phi(0,1) \quad (21)$$

where the constants C_1, C_2, ..., C_8 are again functions of the $a_1^{(i)}$, $a_2^{(i)}$, and $a_3^{(i)}$ boundary constants, as well as of the transformed coordinate functions α, β, and γ.

Thus, the local analytical algebraic equation relating the value of the velocity potential at the center of the computational element to its neighboring eight known nodal values has been completely determined.

Computational Procedure

The preceding technique is applied to adjacent grid elements, with the boundary nodal point considered as the interior point. For a general grid element with center at (i,j), the resulting algebraic relation between the center value of the velocity potential and its eight surrounding nodal values is

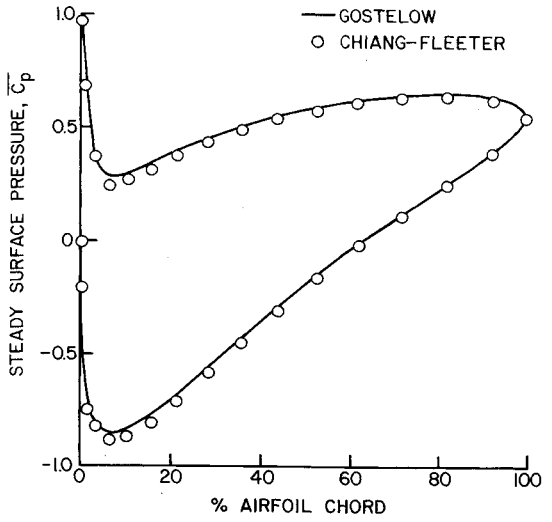

Fig. 6 Correlation of cascade steady prediction and Gostelow solution.

given in Eq. (22):

$$\Phi(i,j) = C_{i+1,j+1}\Phi(i+1,j+1) + C_{i+1,j}\Phi(i+1,j) + C_{i+1,j-1}\Phi(i+1,j-1) + C_{i,j-1}\Phi(i,j-1) + C_{i-1,j-1}\Phi(i-1,j-1) + C_{i-1,j}\Phi(i-1,j) + C_{i-1,j+1}\Phi(i-1,j+1) + C_{i,j+1}\Phi(i,j+1) \quad (22)$$

where $2 \le i \le i_{\max} - 1$, $2 \le j \le j_{\max} - 1$, and C_{ij} are functions of the $a_1^{(i)}$, $a_2^{(i)}$, and $a_3^{(i)}$ boundary constants as well as the transformed coordinate functions α, β, and γ.

The global boundary conditions are specified in Eqs. (23):

$\Phi(i,1)$ = airfoil and wake boundary conditions

$$1 \le i \le i_{\max} \quad (23a)$$

$\Phi(i,j_{\max})$ = farfield inlet and cascade periodic boundary conditions

$$1 \le i \le i_{\max} \quad (23b)$$

$\Phi(i_{\max},j)$ = farfield exit boundary conditions

$$1 < j < j_{\max} \quad (23c)$$

$\Phi(1,j)$ = farfield exit boundary conditions

$$1 < j < j_{\max} \quad (23d)$$

These global boundary conditions, together with the interior point solution specified in Eq. (22) for $\Phi(i,j)$, where $2 \le i \le i_{\max} - 1$, and $2 \le j \le j_{\max} - 1$, lead to a system of algebraic equations. For a fixed j value,

$$-C_{i-1,j}\Phi(i-1,j) + \Phi(i,j) - C_{i+1,j}\Phi(i+1,j) = C_{i+1,j+1}\Phi(i+1,j+1) + C_{i-1,j+1}\Phi(i-1,j+1) + C_{i,j+1}\Phi(i,j+1) + C_{i+1,j-1}\Phi(i+1,j-1) + C_{i-1,j-1}\Phi(i-1,j-1) + C_{i,j-1}\Phi(i,j-1) \quad (24)$$

The right-hand side of this equation is comprised of known quantities; i.e., the $(j-1)$ terms are known from the bound-

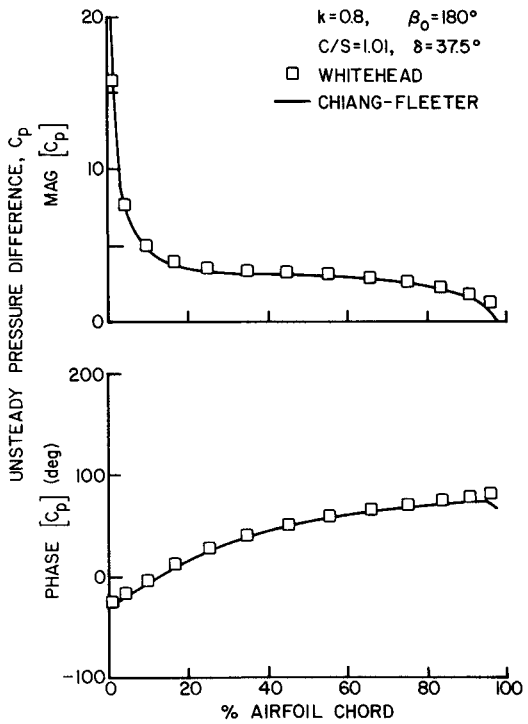

Fig. 7 Correlation of cascade unsteady prediction and Whitehead solution.

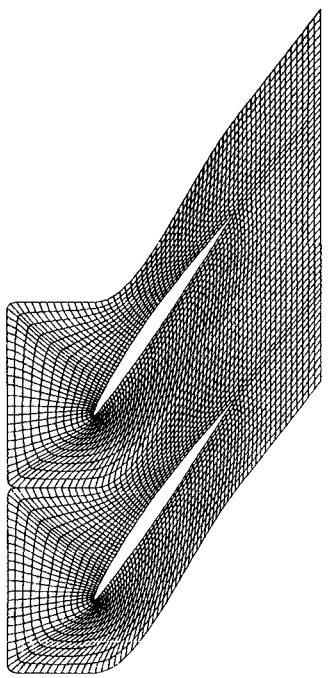

Fig. 8 Computational grid for Unsteady Cascade Standard Configuration 1.

ary conditions ($j=2$) or the last sweep, with the ($j+1$) terms determined from the boundary condition ($j=j_{max}-1$) or the previous iteration.

Equation (24) can be written as a tridiagonal matrix, with the matrix solved by Thomas algorithm for all j values ($2\leq j\leq j_{max}-1$). This procedure is then iterated by successive over-relaxation until the entire solution converges.

Results

A complete first-order model and locally analytical solution have been developed to analyze the oscillating incompressible

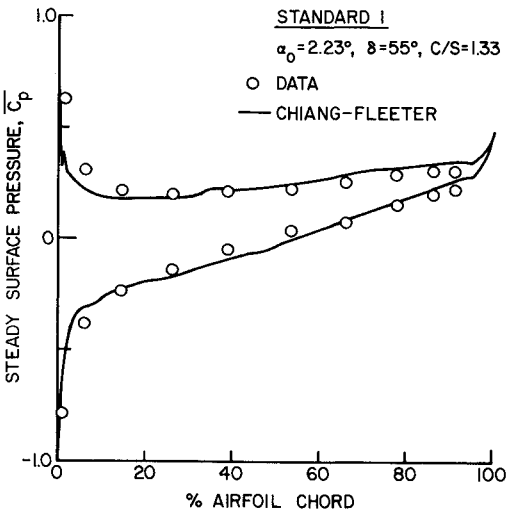

Fig. 9 Steady Standard Configuration 1 data correlation.

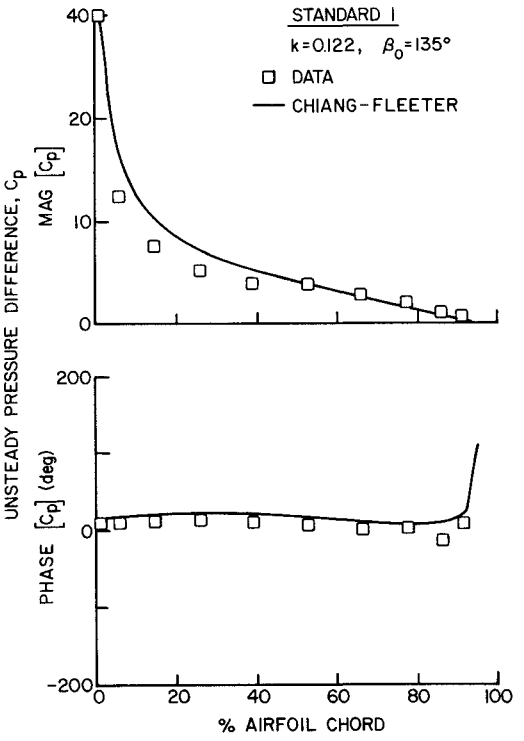

Fig. 10 Unsteady Standard Configuration 1 correlation, $\beta_0=135$ deg.

aerodynamics of a cacade comprised of cambered, thick airfoils. The steady flow is independent of the unsteady flowfield. However, the unsteady flow is coupled to the steady flowfield through the boundary conditions on the airfoil surfaces. Thus, valid steady flow solutions are required to predict accurately the unsteady aerodynamics of an oscillating airfoil cascade.

To demonstrate the steady flow predictive capability of this model and locally analytical solution, the theoretical cascade initially considered by Gostelow[9] is analyzed. This cascade, shown in Fig. 3, is characterized by a stagger angle of 37.5 deg, a solidity of 1.01, and a mean flow incidence angle of 1.0 deg. Predictions for the noncirculatory, circulatory, and total velocity potentials are presented in Fig. 5. The correlation of the predicted chordwise distribution of the airfoil surface static pressure coefficient $\bar{C}_p$, obtained with the model developed herein, with that of Gostelow is shown in Fig. 6. As seen, there is very good correlation between the two analyses.

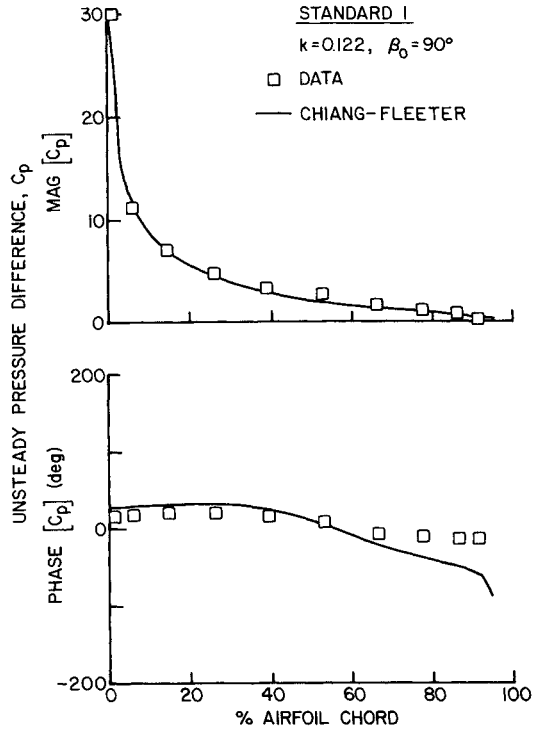

Fig. 11 Unsteady Standard Configuration 1 correlation, $\beta_0 = +90$ deg.

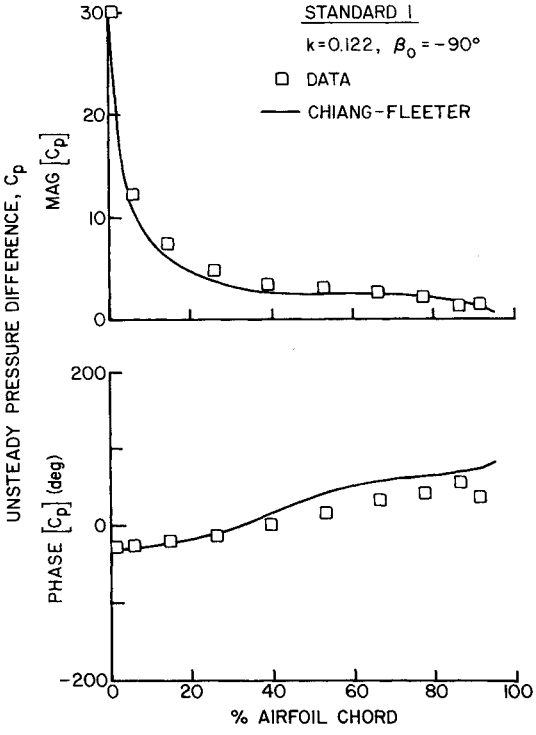

Fig. 12 Unsteady Standard Configuration 1 correlation, $\beta_0 = -90$ deg.

To verify the unsteady oscillating cascade modeling and solution, unsteady predictions are correlated with those from the classical model of Whitehead.[10] In particular, a flat-plate airfoil cascade with a solidity of 1.01 and a stagger angle of 37.5 deg, executing harmonic torsion mode oscillations at a reduced frequency of 0.8 with a 180-deg interblade phase angle, is considered. The resulting predictions from the two models for the chordwise distribution of the unsteady surface

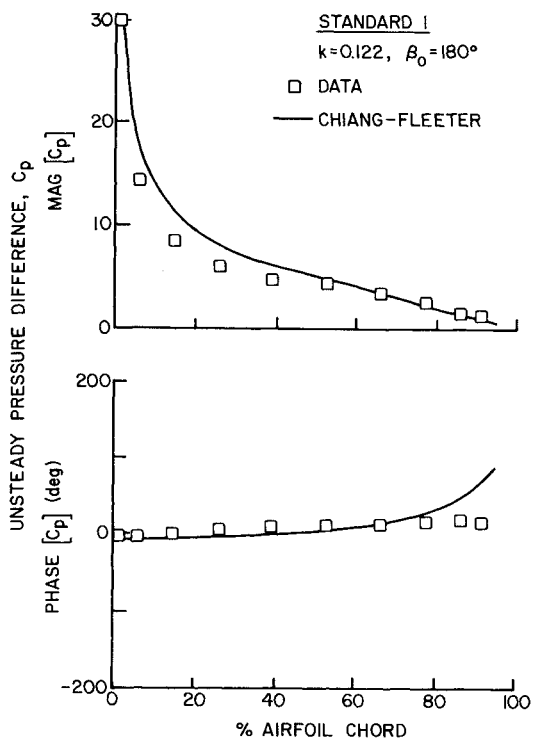

Fig. 13 Unsteady Standard Configuration 1 correlation, $\beta_0 = 180$ deg.

pressure difference C_p are presented in Fig. 7. The excellent agreement between the two analyses is clearly seen.

The capabilities and validity of this model and solution technique are demonstrated by applying it to two appropriate well-documented experimenal test cases. In particular, predictions are correlated with 1) steady and harmonically oscillating unsteady data obtained by Carta,[11,12] for Turbomachine Aeroelasticity Standard Configuration Number 1; Compressor Cascade in Low Subsonic Flow; and 2) unsteady airfoil surface pressure difference data obtained in the NASA Lewis Transonic Oscillating Cascade Facility.[13]

The Turbomachine Aeroelasticity Standard Configuration cascade of Carta is comprised of 11 NACA 65-Series airfoils in an incompressible flow oscillating in torsion about a midchord elastic axis at a reduced frequency of 0.122. The solidity and stagger angle of the cascade are 1.33 and 55 deg, respectively. The airfoils each have a chord of 0.1524 m, a span of 0.254 m, 10-deg circular arc camber, and a thickness-to-chord ratio of 0.06. Figure 8 depicts the flow configuration as well as the computational grid for this cascade.

The predicted and measured chordwise distributions of the airfoil surface steady static pressure at 2.23 deg of incidence are presented in Fig. 9. Very good correlation exists, with the possible exception of the leading edge region on the suction surface. Figures 10–13 show the correlation of the airfoil surface unsteady pressure differences with the cascade oscillating at a reduced frequency of 0.122 for both forward and backward traveling waves. In particular, for interblade phase angles of 135, 90, −90, and 180 deg at 2.23 deg of incidence, the magnitude and phase of the unsteady pressure difference data and the corresponding prediction are presented. The very good correlation between the predictions and the data is readily apparent.

The second data set considered was obtained in experiments at NASA Lewis, in which the unsteady surface pressure difference was measured on an oscillating cascade in a subsonic compressible flow. The cascade consists of nine symmetric, uncambered, biconvex airfoils with a chord of 7.62 cm, a thickness-to-chord ratio of 0.076, a solidity of 1.3, and a

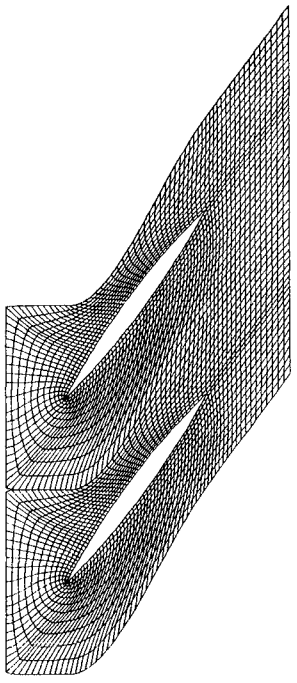

Fig. 14 Computational grid for NASA Lewis flutter cascade.

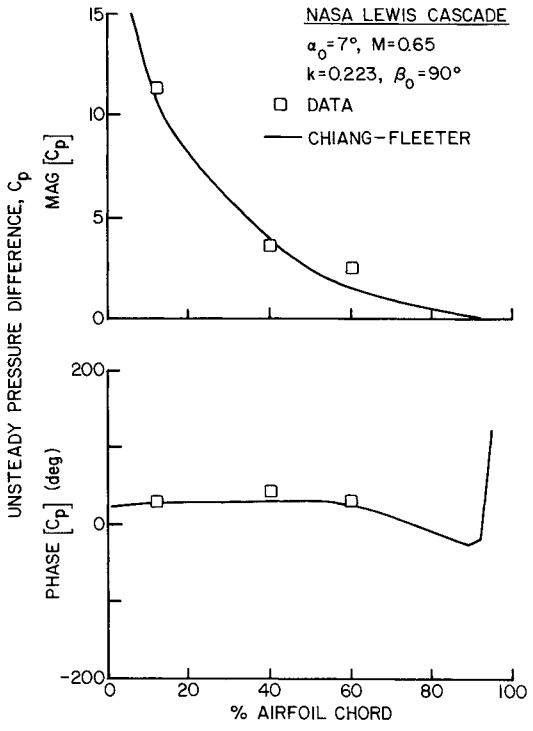

Fig. 15 NASA Lewis flutter cascade correlation, $\beta_0 = +90$ deg.

53-deg stagger angle. The computational grid utilized for the predictions from the model developed herein as well as the airfoil and cascade flow geometry are shown in Fig. 14.

With an inlet Mach number of 0.65 and the cascade set at 7 deg of incidence, the airfoils were oscillated in torsion about a midchord elastic axis at a reduced frequency of 0.223. Data obtained defined the unsteady airfoil surface pressures at interblade phase angles of 90, 0, and −90 deg. These data, together with the predictions from this incompressible model and locally analytical solution, are presented in Figs. 15–17. Both the unsteady pressure magnitude and phase data exhibit very good correlation with the predictions for these interblade phase angle values.

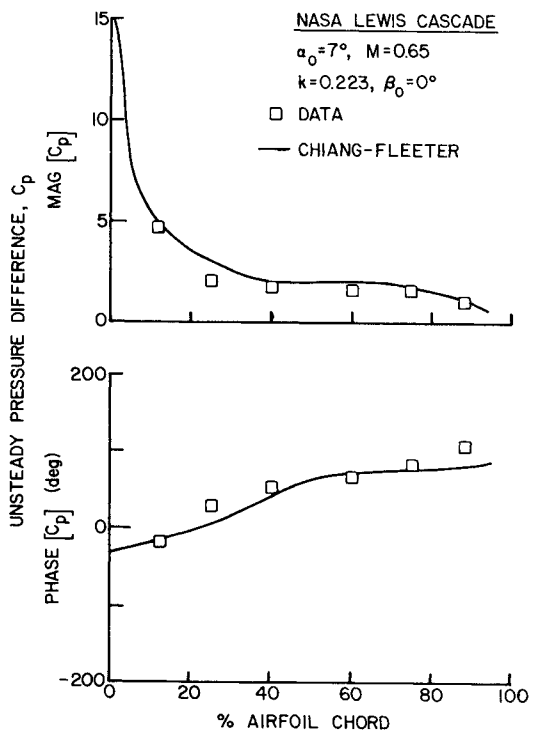

Fig. 16 NASA Lewis flutter cascade correlation, $\beta_0 = 0$ deg.

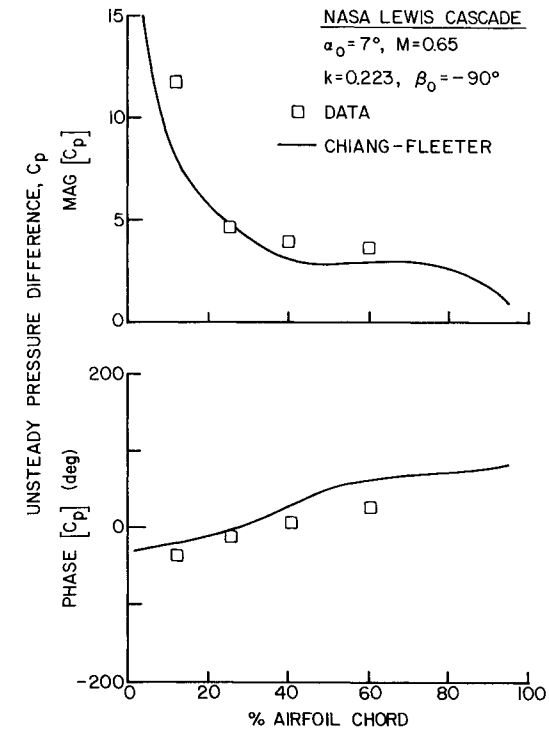

Fig. 17 NASA Lewis flutter cascade correlation, $\beta_0 = -90$ deg.

Summary and Conclusions

A complete first-order model has been developed to predict the oscillating incompressible aerodynamics of an airfoil cascade, including the effects of steady aeodynamic loading, i.e., airfoil profile, cascade geometry, and mean flow incidence angle. The cascade steady and unsteady flowfields are analyzed by considering a single flow channel with periodic boundary conditions. The velocity potential is separated into

steady and unsteady harmonic components, which are individually described by Laplace equations. The steady velocity potential is independent of the unsteady flowfield. However, the unsteady flow is coupled to the steady flowfield through the boundary conditions on the surfaces of the oscillating airfoil.

Solutions for both the steady and unsteady flowfields are obtained by a locally analytical solution method. In this method, the discrete algebraic equations that represent the flowfield equations are obtained from analytical solutions in individual grid elements of a body-fitted computational grid, with the complete solution determined by assembling these locally analytical solutions.

The capabilities and validity of this model and locally analytical solution were then demonstrated by predicting the steady and unsteady aerodynamics of both theoretical and experimental cascade configurations. In particular, very good correlation between the predictions from this model and solution technique were obtained with 1) Gostelow's steady cascade flowfield prediction, 2) the oscillating flat plate cascade model of Whitehead, 3) the steady and oscillating cascade unsteady data of Turbomachine Aeroelasticity Standard Configuration Number 1: Compressor Cascade in Low Subsonic Flow; and 4) the unsteady airfoil surface pressure difference data obtained in the NASA Lewis Transonic Oscillating Cascade Facility.

Acknowledgment

This research was sponsored in part by the Air Force Office of Scientific Research and the NASA Lewis Research Center.

References

[1]Hanamura, Y., "Flutter of Cascading Blade Row," 1st Rept., *Institute of Space and Aeronautical Science, University of Tokyo, Report No. 459*, Vol. 36, No. 1, 1971, pp. 1-36.

[2]Hanamura, Y., "Flutter of Cascading Blade Row," 2nd Rept., *Institute of Space and Aeronautical Science, University of Tokyo, Rept. No. 503*, Vol. 38, No. 14, 1973, pp. 405-420.

[3]Atassi, H., and Akai, T. J.,"Aerodynamic and Aeroelastic Characteristics of Oscillating Loaded Cascades at Low Mach Number," American Society of Mechanical Engineers, New York, Paper 79-GT-111, 1979.

[4]Chen, C. J., Naseri-Neshat, H., and Ho, K. S., "Finite Analytic Numerical Solution of Heat Transfer in Two-Dimensional Cavity Flow," *Journal of Numerical Heat Transfer,* Vol. 4, No. 2, April-June 1981, pp. 179-197.

[5]Chen, C. J. and Yoon, Y. H., "Finite Analytic Numerical Solution of Axisymmetric Navier-Stokes and Energy Equations," *Journal of Heat Transfer,* Vol. 5, Aug. 1983, pp. 639-645.

[6]Chen, C. J. and Li, P., "Finite Differential Methods in Heat Conduction—Application of Analytic Solution Techniques," American Society of Mechanical Engineers, New York, Paper 79-WA/HT-50, Dec. 1979.

[7]Chen, C. J. and Li, P., "The Finite Analytic Method for Steady and Unsteady Heat Transfer Problems," American Society of Mechanical Engineers, New York, Paper 80-HT-86, 1980.

[8]Moore, R. M., "Numerical Solutions of Unsteady Inviscid Transonic Turbine Cascade Flows," Ph.D. Thesis, Purdue Univ., Lafayette, IN, May 1988.

[9]Gostelow, J. P., *Cascade Aerodynamcis,* Pergamon, New York, 1984.

[10]Whitehead, D. S., "Force and Moment Coefficients for Vibrating Airfoils in Cascade," Aeronautical Research Council, London, R&M 3254, 1962.

[11]Bolcs, A. and Fransson, T. H., "Aeroelasticity in Turbomachines—Comparison of Theoretical and Experimental Cascade Results," *Communication Du Laboratoire de Thermique Appliquee et de Turbomachines Number 13,* Ecole Polytechnique Federale de Lausanne, Switzerland, 1986.

[12]Carta, F. O., "Unsteady Gapwise Periodicity of Oscillating Cascaded Airfoils," American Institute of Mechancial Engineers, New York, Paper 82-GT-286, 1982.

[13]Buffum, D. R., Boldman, D. R., and Fleeter, S., "The Unsteady Aerodynamics of an Oscillating Cascade in a Compressible Flow Field," *4th International Symposium on Unsteady Aerodynamics and Aeroelasticity of Turbomachines and Propellers,* Aachen, FRG, Sept. 1987.